BBA - Molecular and Cell Biology of Lipids 1865 (2020) 158715

Contents lists available at ScienceDirect

BBA - Molecular and Cell Biology of Lipids

journal homepage: www.elsevier.com/locate/bbalip

Expression of the type 1 lysophosphatidic acid receptor in osteoblastic cell lineage controls both bone mineralization and osteocyte specification☆

Candide A. Alioli[a,1], Léa Demesmay[b,1], Sara Laurencin-Dalacieux[a], Nicolas Beton[a], Delphine Farlay[b], Helene Follet[b], Amri Saber[a], François Duboeuf[b], Jerold Chun[c], Richard Rivera[c], Daniel Bouvard[d], Irma Machuca-Gayet[b], Jean-Pierre Salles[a], Isabelle Gennero[a,2], Olivier Peyruchaud[b,*,2]

[a] Centre de Physiopathologie de Toulouse Purpan INSERM UMR 1043, Toulouse, France
[b] Pathophysiology, Diagnosis and treatments of bone diseases, INSERM UMR1033, Lyon, France
[c] Sanford Burnham Prebys Medical Discovery Institute, La Jolla, CA 90237, USA
[d] Institute for Advance Biosciences, Grenoble, France

ARTICLE INFO

Keywords:
Lpar1
LPA_1
Osteoblast
Osteocyte
Bone
Knockout mice

ABSTRACT

Lysphosphatidic acid (LPA) is a major natural bioactive lipid mediator whose biological functions affect multiple organs. These include bone as demonstrated by global *Lpar1*-knockout mice (*Lpar1*$^{-/-}$) which present a bone growth defect. LPA acts on all bone cells including osteoblasts, that are responsible for bone formation, and osteoclasts, which are specialized cells that resorb bone. LPA appears as a potential new coupling molecule during bone remodeling. LPA_1 is the most ubiquitous LPA receptor among the six LPA receptor family members (LPA_{1-6}). To better understand the specific role of LPA *via* its receptor LPA_1 in osteoblastic cell lineage we generated osteoblast-specific *Lpar1* knockout mice (*Lpar1*-ΔOb) by crossing *Lpar1*$^{flox/flox}$ and Osx:Cre^{+} mouse lines. *Lpar1*-ΔOb mice do not recapitulate the bone defects of *Lpar1*$^{-/-}$ mice but revealed reduced bone mineralization and decreased cortical thickness, as well as increased bone porosity associated with an augmentation in the lacunae areas of osteocyte and their apoptotic yield. *In vitro*, primary *Lpar1*-ΔOb and immortalized cl1-Ob-*Lpar1*$^{-/-}$ osteoblasts revealed a remarkable premature expression of alkaline phosphatase, reduced cell proliferation associated with decreased YAP-P nuclear accumulation, and reduced mineralization activity. Osteocyte specification is markedly impaired as demonstrated by reduced expression of early (E11) and late (DMP1, DKK1, SOST) osteocyte markers *ex vivo* in enriched osteocytic fractions of *Lpar1*-ΔOb mouse bone explants. In addition, E11 expression and dendrite formation induced by FGF2 are markedly impaired in both primary *Lpar1*-ΔOb and immortalized cl1-Ob-*Lpar1*$^{-/-}$ osteoblasts. Taken together these results suggest a new role for LPA in bone mass control *via* bone mineralization and osteocyte function.

Abbreviations: ALP, Alcaline phosphatase; Bglap, Osteocalcine; BMSC, Bone marrow mesenchymal cells; BSA, Bovine serum albumin; BSP, Bone sialoprotein; BV/TV, Bone volume over tissue volume ratio; CFU-F, colony-forming-unit-fibroblasts; Col1, Collagen 1; Cre, Cre recombinase; CTRL, Control; Cx43, Connexin 43; Dkk1, Dikkopf-related -protein-1; DMEM, Dulbecco's modified Eagle's medium; Dmp1, Dentin matrix protein 1; E11, Podoplanin; FBS, Foetla calf serum; FGF-23, Fibroblast growth factor 23; FGF2, Fibroblast growth factor 2; FTIRM, Fourier transform infrared microspectroscopy; GAPDH, Glyceraldehyde-3-phosphate dehydrogenase; GFP, Green fluorescent protein; HBSS, Hank's balanced salt solution; Lats1/2, Large Tumor Suppressor Kinase 1/2; LDH, Lactate dehydrogenase; LPA, Lysophosphatidic acid; LPA1–6, LPA receptor 1–6; Lpar1, LPA receptor gene; Mepe, Matrix extracellular phosphoglycoprotein; MicroCT, Micro-computed tomography; MSC, Mesenchymal cells; MSD, Musculoskeletal diseases; Ob, Osteocblast; Opn, Osteopontin; Osx, Osterix; PBS, Phosphate buffer; PFA, Paraformaldehyde; PHEX, phosphate regulating endopeptidase homolog X-linked; PMMA, Polymethyl methacrylate; Ppargc1a/b, Peroxisome proliferator-activated receptor gamma coactivator 1-alpha/beta; qRT-PCR, Quantitative reverse transcription-polymerase chain reaction; Runx2, Runt-related transcription factor 2; SOST, Sclerostin; TAZ, Transcriptional co-activator with PDZ-motif; TBP, TATA-Box Binding Protein; YAP, Yes-associated protein 1

☆ This article is part of a Special Issue entitled Lysophospholipids and their receptors: New data and new insights into their function edited by Susan Smyth, Viswanathan Natarajan and Colleen McMullen.

* Corresponding author.
E-mail address: olivier.peyruchaud@inserm.fr (O. Peyruchaud).

[1] indicates persons who contributed equally to this work.
[2] indicates persons who contributed equally to this work.

https://doi.org/10.1016/j.bbalip.2020.158715
Received 5 March 2020; Received in revised form 3 April 2020; Accepted 10 April 2020
Available online 21 April 2020
1388-1981/

1. Introduction

Musculoskeletal diseases (MSD) are the most common disorders in the human population [1]. MSD have a paramount social and economic consequences because they exacerbate the impact of multimorbidity [2]. This indicates the need for better clinical care for patients with bone diseases. Bone is a complex tissue whose integrity is maintained throughout the life by the continuous process of bone remodeling [3]. This process is controlled by two cell types: osteoclasts that resorb bone, and osteoblasts that form new bone. Crosstalk and exchanges between these cells, under the influence of mechanical stimulation, immune cell action, and both paracrine and endocrine growth factors, control bone remodeling. Impaired coordination between osteoblasts and osteoclasts leads to an imbalance of bone remodeling that is responsible for multiple forms of MSD.

Lysophosphatidic acid (LPA) is a naturally occurring bioactive lipid with growth factor activity on a wide range of cells [4]. LPA's effects are mediated by six different G protein-coupled receptors ($LPA_{1–6}$). These receptors share intracellular signaling pathways dependent on $G\alpha_i$ ($LPA_{1,4,6}$), $G\alpha_{12/13}$ ($LPA_{1,2,4,6}$), $G\alpha_q$ ($LPA_{1,5}$) and $G\alpha_S$ ($LPA_{4,6}$) resulting in potentially redundant or opposing effects of LPA receptors on cell biology, which include cytoskeleton rearrangements, cell motility, survival, and both proliferation and differentiation [5]. Evidence that LPA is produced within bone tissue has been obtained in the context of bone metastasis wherein it acts as a paracrine factor stimulating cancer cell proliferation, cytokine secretion and osteoclastic bone resorption [6,7]. The therapeutic use of LPA and LPA derivatives in bone regeneration has been proposed recently [8]. However, most eukaryotic cells, including bone cells, express various forms of LPA receptors [9–11]. As a consequence, activation of different cell types in bone may undermine the complex mode of action of LPA in bone pathophysiology due to pleiotropic activities of LPA through co-activation signals from multiple receptors. Understanding the role of each type of LPA receptor in bone cell functions *in situ* is crucial for more effective therapeutic applications in MSD.

LPA_1 is the most ubiquitous LPA receptor in mammalians [12]. Global deletion of the LPA_1 gene in mice (*Lpar1*) and zebrafish (lpa_1) alters the growth of animals as a consequence of chondrocyte proliferation and bone formation defects [9,13]. However, analyses of the $Lpar1^{-/-}$ mouse global phenotype have revealed a large spectrum for LPA function in general homeostasis. $Lpar1^{-/-}$ mice have major neurological defects [14] with an additional alteration in olfactive bulb maturation that markedly impairs food intake [15]. These mice also exhibit adipogenesis and glucose tolerance defects [16]. Bone development is very sensitive to metabolic changes such as those that occur in obesity and diabetes [17]. The dietary deficiencies and poor metabolic regulation observed in $Lpar1^{-/-}$ mice are therefore likely to compromise bone homeostasis. Furthermore, LPA_1 is expressed in almost all cell types present in the bone microenvironment, osteoblasts [9], osteoclasts [10], osteocytes [11], chondrocytes [13] and adipocytes [16]. Thus, the bone phenotype of $Lpar1^{-/-}$ mice is likely to be a consequence of multiple constraints on bone remodeling.

In order to evaluate the specific role of LPA_1 expressed by osteoblasts during bone development we generated Osx-Cre:GFP/$Lpar1^{fl/fl}$ ($\Delta LPA_1{}^{Osx}$) mice that exhibited tissue-specific deletion of *Lpar1* in osteoblastic cell lineage. Micro-computerized tomography measurements, bone histology and confocal microscopy analyses of $\Delta LPA_1{}^{Osx}$ mice associated with primary and immortalized $\Delta LPA_1{}^{Osx}$ bone cell biology investigations revealed that osteoblastic expression of LPA_1 controls bone quality through osteocyte behavior but not bone growth.

2. Materials and methods

2.1. Mice

Mice with a specific deficiency of *Lpar1* in the osteoblastic cell lineage (*Lpar1*ΔOb) were generated by using the Cre/loxP strategy. C57B6J carrying loxP sites flanking exon 3 of the LPA_1 receptor gene, $Lpar1^{fl/fl}$ mice, recently generated by J. Chun and R. Rivera [18] were crossed with BALB/c heterozygous mice expressing Cre-recombinase driven by the osterix promoter (Osx1-GFP::Cre/+ mice) obtained from Dr. Andrew P. McMahon, Harvard University, Cambridge, USA [19].

2.2. Ethics statement

Mice were housed in pathogen-free conditions in the Experimental Therapy Units in Toulouse (INSERM US 006 ANEXPLO/CREFRE) in accordance with the Guide for the Care and Use of Laboratory Animals of the European Council and under the supervision of the authorized investigators. All protocols involving animal experimentations were approved by the Animal Care and Ethics Committee of US006/CREFE (CEEA-122; application number APAFIS#5122–20,160,420 17,274,859 v2).

2.3. Mouse genotyping and real-time PCR

The genotype of all experimental mice was determined by PCR analysis of genomic DNA extracted from tail or ear biopsies using the following primers: Cre transgene: forward 5'-CCTGGAAAATGCTTCTG TCCGTTTGCC-3′ and reverse: 5'-GAGTTGATAGCTGGCTGGTGGCAG ATG-3′; *Lpar1* allele: 5'LoxP forward: 5'-GTTGGGACATGGATGCTA TTC-3′, Internal forward 1: 5'-AGACTGTGGTCATTGTGCTTG-3′, 3'LoxP reverse: 5'-GGTTTAGTGGTGTGGGATCG-3′. Total RNA from OC cultures and from powdered whole bone was extracted using Trizol (Invitrogen AB) and the Nucleospin RNAII kit (Macherey-Nagel). Complementary DNA from OC and bones were synthesized by reverse transcription using the iScript cDNA Synthesis kit (Biorad), Expression of target genes was quantified by qRT-PCR using the Biorad CFX Connect Real Time PCR Detection System with the iTaq Universal SYBR Green Supermix (Biorad) and sets of specific primers. Quantifications were normalized to TBP values and expressed as relative expression using the 2(−Delta Delta C(T)) method (27). Primer sequences are indicated in Table 1.

2.4. Micro-computed tomography (μCT)

Three-dimensional (3D) microarchitecture of the distal metaphyseal femur and cortical midshaft were carried out using a Skyscan 1176 micro-CT scanner (Skyscan Inc.). The X-ray excitation voltage was set to 50 kV with a current of 500 mA. A 0.5 mm aluminum filter was used to reduce beam-hardening artifacts. Samples were scanned in 70% ethanol with a fixed voxel size of 9.08 μm. Section images were reconstructed with NRecon software (version 1.6.1.8, Skyscan). The region of interest to delineate trabecular bone was drawn manually away from the endocortical surface, starting at 0.3 mm of underneath the growth plate and ending at 1.3 mm. For cortical analysis, 0.5 mm on either sides of the femur midshaft were reconstructed. The global threshold was set at 0.394 g HA/cm^3. Three-dimensional modeling and analysis of bone, vertebra length and bone volume to tissue volume (BV/TV) were obtained with the CTAn (version 1.9) and CTVol (version 2.0) softwares.

2.5. Digitized microradiography

The technique of digitized microradiography was used to measure the degree of mineralization of bone (DMB) and its heterogeneity index [20]. Briefly, 50 μm-thick bone sections were analyzed with a Hammamatsu L9421–02 Microfocus X-ray system tube with a power maximum of 8 W, a copper anode, a nickel filter, a beryllium window of 150 μm and a focal spot size of 5 μm in diameter. The exposure parameters were high voltage: 40 kV, current: 50 μA, and power of 2 W. The detector was a Photonic Science FDI VHR 11 M CCD camera with an active area of 36 × 24 mm (4008 × 2671 pixels). The scintillator was

Table 1
List of primer sequences.

Target	Forward (5′-3′)	Reverse (5′-3′)
Lpar1	CCAGGAGGAATCGGGACAC	CAATAACAAGACCAATCCCGGA
Lpar2	GTCAAGACGGTTGTCATCATTCT	GAAGCATGATCCGCGTGCT
Lpar3	ACAAAGCTTGTGATCGTCCTGT	TCATGATGGACATGTGTCTTTCC
Lpar4	GCATTGTTGACATTAGTGGTGGA	AACCTGGCCCTCTCTGATTT
Lpar5	CCGTACATGTTCATCTGGAAGAT	CAGACTAATTTCTCTTCCCACCT
Lpar6	TGGCATATGGCTGTCACCTA	GGGGATTCTGCACAAGTGAT
Alpl	CGGATCCTGACCAAAAACC	TCATGATGTCCGTGGTCAAT
Bsp2	GAAAATGGAGACGGCGATAG	CATTGTTTTCCTCTTCGTTTGA
Col1	GCCTTGGAGGAAACTTTGCTT	CACGGAAACTCCAGCTGATTTT
Dkk1	CCGGGAACTACTGCAAAAAT	CCAAGGTTTTCAATGATGCTT
Dmp1	CATTCTCCTTGTGTTCCTTTGG	TCAGTATTGTGGTATCTGGCAACT
E11	GCCAGTGTTGTTCTGGGTTT	TCTCCTGTACCTGGGGTCAC
Cx43	GTGCCGGCTTCACTTTCA	GGAGTAGGCTTGGACCTTGTC
Mepe	GATGCAGGCTGTGTCTGTTG	TCCTGTCTTCATTCGGCATT
Bglap	AGACTCCGGCGCTACCTT	CTCGTCACAAGCAGGGTTAAG
Opn	GGAAACCAGCCAAGGTAAGC	TGCCAATCTCATGGTCGTAG
PHEX	CTGCCAGAGAACAAGTGCAA	AATGGCACCATTGACCCTAA
SOST	TCCTGAGAACAACCAGACCA	GCAGCTGTACTCGGACACATC
TBP	TCTGAGAGCTCTGGAATTGTACCG	TGATGACTGCAGCAAATCGCTTG

Gd2O2S:Tb, and an aluminum filter of 12 μm was used. The image digitization step was made with a 12-bit digital image detector (pixel size: 9 μm, object pixel size: 0.83 μm). A threshold of 0.8 g/cm3 was used. The mean DMB were expressed in g mineral/cm^3. Cortical porosity was measured on X-ray images with ImageJ software. A threshold was applied (Li method) and the thresholded image then was then segmented outline selected. The cortical porosity was assessed using weighting by the total number of pixels analyzed. For the quantification of the sizes of pores, each pore was automatically outlined and identified by a digit. Areas of pores were expressed in μm square (μm2). The size of the different pores was measured and the distribution of the sizes of their size was generated.

2.6. Fourier transform infrared microspectroscopy (FTIRM)

Analysis of the intrinsic material properties of bone was performed on cortical bone as previously described [21,22]. Briefly, thin bone sections from blocks embedded in PMMA (2 μm thick) were longitudinally cut with a polycut in proximal tibia, and analyzed in transmission mode with a Perkin-Elmer GXII Auto-image Microscope (Norwalk, CT, USA) equipped with a wide band detector (mercury-cadmium-telluride; 7800–400 cm^{-1}). A Cassegrain objective with a numerical aperture of 0.6 was used with a spatial resolution of 10 μm at typical mid-infrared wavelengths. Ten areas (50 μm × 50 μm) in metaphysis and 10 in diaphysis were scanned. After curve-fitting of infrared spectra, 4 variables were measured: mineral maturity, crystallinity, mineral/organic ratio, and collagen maturity. Each spectrum was collected at 2 cm^{-1} resolution, and 40 scans by spectrum were performed in the transmission mode. The contributions of air and PMMA were subtracted from the original spectrum, baseline adjusted and curve-fitted with Python software [23]. The following parameters were determined: the mineral crystallinity (cryst), which is inversely proportional to the full width at half-maximum of the 604 cm^{-1} peak (apatite phosphate environment ν_4PO_4) and corresponds to both crystal size and perfection [22], the mineral to organic ratio (min/org) *i.e.* the area ratio of the bands of mineral matrix over organic matrix (1184–910 cm^{-1}/1712–1592 cm^{-1}) [24], the mineral maturity (min mat) which is calculated as the area ratio of the apatite phosphate over non-apatite phosphate (1030/1110 cm^{-1} area ratio) and reflects the age of mineral [22], and the collagen maturity (coll mat) which is calculated as the ratio of organic matrix bands (1660/1690 cm^{-1} area ratio) [21]. Results are expressed as mean ± standard deviation (SD).

2.7. Quantification of YAP nuclear localization

Cells were immunostained as recently described [25] with an anti YAP and images acquired with a confocal laser scanning microscope (Zeiss LSM510) equipped with a 63× plan-Apochromat oil immersion objective (n.a. 1.4) and a pinhole set to one Airy. On each cell image, a region of interest (ROI) was defined either within the nucleus, or in the cytoplasmic area next to the nuclear envelope. As the ROI thickness in the two positions was likely to be identical, the average fluorescence intensity should be proportional to YAP concentration in that area and was estimated using the Fiji public software. Within the same cell, the ratio of the fluorescence intensities in the nucleus *versus* the cytoplasmic area reflects the YAP concentration ratio in the two compartments. This ratio was represented with a logarithmic scale to have an identical range of positive and negative ratios. Measurements were performed with $n \geq 50$ (unless otherwise indicated) and differences were compared with the Student's *t*-test. Boxplots were generated with the R public software.

2.8. Quantification of Rac1 localization

Cells were immunostained with an anti Rac1 and images acquired with a confocal laser scanning microscope (Zeiss LSM510) equipped with a 63× plan-Apochromat oil immersion objective (n.a. 1.4) and a pinhole set to one Airy. On each cell image, a line profiling was acquired using Fiji software. Cell border was defined and used to set the origin. Measurements were performed with $n \geq 50$ and differences were compared with the Student's *t*-test.

2.9. Cell cultures and FGF2 experimental procedure

Mouse BMSC were isolated from the bone marrow of femurs and tibias of control and *Lpar1*ΔOb mice as previously described [26]. Cells were maintained in Alpha Modified Eagle's Medium alpha (αMEM) with 10% (*v*/v) FBS, 100 U/ml penicillin and 0.1 mg/ml streptomycin at 37 °C. For the colony-forming-unit assay, nucleated cells from the bone marrow were seeded at 6 × 10^5 cells per cm^2 and cultured for up to 14 days in the same medium, additionally supplemented with ascorbic acid (50 μg/ml) and beta-glycerophosphate (10 mM).

Control and *Lpar1*ΔOb mice primary osteoblasts were isolated as previously described [27] and maintained in Dulbecco's Modified Eagle's Medium (DMEM) with 100 U/ml penicillin and 0.1 mg/ml streptomycin at 37 °C. Ob-*Lpar1*$^{fl/fl}$ and cl1-Ob-*Lpar1*$^{-/-}$ immortalized osteoblast were cultured in αMEM with 10% (*v*/v) heat inactivated FBS,

100 U/ml penicillin and 0.1 mg/ml streptomycin. For induction of osteogenic differentiation, Ob-*Lpar1* $^{fl/fl}$ and cl1-Ob-*Lpar1* $^{-/-}$ cells were seeded and cultured until they reached confluence. The medium was then supplemented (day 0) with ascorbic acid (50 μg/ml) and beta-glycerophosphate (10 mM) for 21–30 days. For induction of osteocytogenesis, primary and immortalized osteoblasts were seeded, then at the subconfluence (day 0), the culture media were replaced with 1% (*v/v*) FBS supplemented medium, and 10 ng/ml FGF2 (bFGF, Thermo Fisher Scientific) in 0.1% bovine serum albumin (BSA). Cells were treated with FGF2 or 0.1% BSA as vehicle and harvested after 4 h for RT-qPCR analysis or after 24 h for western blot analysis using a mouse podoplanin antibody (R&D Systems). For actin filament visualization, the cells were fixed in 4% PFA, rinsed in PBS and permeabilized in 0.1% (*w/v*) triton X-100 (Sigma) in PBS for 15 mins after vehicle or FGF2 challenge for 72 h. The cells were rinsed and incubated with 0.6 unit/mL of Alexa Fluor 488-conjugated phalloidin (Thermo Fisher Scientific) (in PBS with 0.1% BSA) in the dark at RT for 2 h.

2.10. Ex-vivo osteocyte enriched bone preparation

Osteocytes enriched samples were obtained following as previously described [28]. Briefly, bone pieces from 4 mice femurs and tibias were harvested and flushed with PBS to eliminate the bone marrow, and the trabecular bones cut and removed. The remaining diaphyses samples were serially digested in α-MEM containing 1 mg/ml of collagenase II (Thermo Fisher Scientific) on a rocking platform at 90 oscillations per min at 37 °C for 30 min. The digestion solution containing osteoblasts, osteoclasts and other peripheral cells was discarded, and the samples were washed in HBSS. This experiment was repeated four more times and the digested samples were rinsed, plated and incubated for 24 h in the primary osteoblast culture medium. Samples were then harvested for RT-qPCR experiments.

2.11. Histology

For histological preparations, the cortical femurs from 3 week old CRTL and *Lpar1*ΔOb mice were isolated, fixed in 4% paraformaldehyde for 24 h, dehydrated in 70% Ethanol and decalcified in 14% EDTA for 3 weeks. The paraffin embedded tissue samples were cut into 5 μm sections and stained with Hematoxylin/eosin and analyzed with a Pannoramic 250 Flash III scanner (3DHISTECH Ltd). For each femur sample, three sections were cut into three independent plans. ImageJ software (NIH) was used to count the number osteocytes per mm^2 and to measure the surface of osteocyte lacunae (in μm^2). Each measure was repeated in four randomly selected areas per plan and the average of the three plans was calculated for each mouse. A TUNEL apoptosis assay was then performed using an *in-situ* Cell Death Detection Kit (Roche, Mannheim, Germany) according to the manufacturer's instructions. TUNEL positive osteocytes (in brown) and the living cells (in blue) were counted in four randomly selected area and the ratio positive/living cells (%) was calculated for each mouse. The presence of cleaved Caspase-3 (Asp175) was examined by immunohistochemistry using a monoclonal rabbit anti-mouse antibody (R&D systems) as primary antibody. A biotinylated goat anti-rabbit (Abcam) was used as secondary antibody, and visualized using the peroxidase-conjugated streptavidin-biotin system (Vectastain). Diaminobenzidine (Abcam) chromogene substrate was used to visualize positive cells as brown and hematoxylin eosin was used as counterstaining. The ratio (%) of positive osteocytes from four randomly selected area was calculated for each mouse with ImageJ software.

2.12. Confocal osteocyte imaging and quantification

30 μm thick cryo sections of decalcified femurs from both genotypes were labeled for 1 h with Alexa Fluor 488 Phalloidin (Life Technologies) and DAPI from (Roche) and then mounted in Fluorsave Reagent (Calbiochem). Image acquisition was performed at high voxel resolution with a Zeiss LSM 880 laser scanning confocal microscope, using an Objective Plan-Apochromat Oil DIC M27. Z stack images were deconvoluted using Huygens Scientific Volume Imaging (B.V. Netherlands) and 3-D reconstruction and dendrite quantification was assessed using Bitplane Imaris 9.3 software (Oxford Instruments).

2.13. Isolation, immortalization, infection, and in vitro Cre-mediated deletion of osteoblasts

Experiments were carried out using the procedure as previously described [29]. Briefly, a primary mouse osteoblast-enriched cell population was isolated from newborn calvaria using a mixture of 0.3 mg/ml collagenase type I (Sigma-Aldrich) and 0.25% trypsin (Invitrogen). Cells were grown in α-MEM medium containing 10% FCS. Primary osteoblasts (passage 2) were immortalized by transduction with a retrovirus expressing the large SV40 T antigen, cloned, and then tested for their ability to induce alkaline phosphatase upon differentiation. *Lpar1* $^{fl/fl}$ immortalized osteoblasts were infected with an adenoviral supernatant encoding the Cre recombinase for 1 h in PBS supplemented with 2% FBS and 1 mM MgCl2.

3. Results

3.1. Selective Lpar1 deletion in osteoblasts affects bone morphometric parameters

Conditional knockout mice for *Lpar1* in the early osteoblastic cell lineage (*Lpar1*ΔOb) were generated by crossing *Lpar1* $^{fl/fl}$ animals [18] with OsxCre $^{+/-}$ mice (CTRL) whose Cre recombinase is driven by the osterix (Osx) promoter [19]. We choose the Osx promoter as a driver for the Cre-recombinase expression because its activation follows Runx2 activation, which engages mesenchymal stem cells into the osteoblastic lineage. *Lpar1* expression was significantly decreased in the bone of *Lpar1*ΔOb mice without affecting the expression of genes coding for any other types of LPA receptors (Fig. 1A). In addition, major tissues that are well-known to express LPA_1 (heart, brain, lungs, intestine) did not show significantly altered expression of *Lpar1* in *Lpar1*ΔOb mice indicating the specificity of our animals for investigating the role of LPA_1 expressed by cells of the osteoblastic lineage on bone development.

Mice with global deletion of *Lpar1* (*Lpar1* $^{-/-}$) revealed an osteoporotic phenotype at 4 weeks of age without significant differences between males and females [9]. Since then, no studies have further characterized the bone phenotype of *Lpar1* $^{-/-}$ mice. We therefore decided to focus our study on one-month-old female mice. *Lpar1*Δ Ob mice showed a mild growth retardation phenotype as judged by a significantly shorter length of the femurs (6% reduction) and smaller size of vertebral plates (11% reduction) compared to controls (Fig. 1C-D). Interestingly, no significant alteration of the bone mass was detected in *Lpar1*Δ Ob mice even though we observed a trend for decreased values of BV/TV (Fig. 1E) and trabecular thickness (Fig. 1F) parameters indicating a marginal impact on trabecular bone remodeling (Fig. 1 D). By contrast, femur cortical bone thickness was significantly decreased in *Lpar1*Δ Ob mice as compared to CTRL mice (Fig. 1F-G).

3.2. Altered osteoblast differentiation and defective mineralization in Lpar1Δ Ob mice

To investigate the impact of Lpar1 osteoblast selective deletion at the cellular level, bone marrow MSCs (mesenchymal stem cells) were derived from CRTL or *Lpar1*ΔOb mice, and cultured under osteogenic conditions. *Lpar1*ΔOb cultures displayed a lower number and size of fibroblastic methylene blue stained colonies than CTRL, suggesting a defect in early progenitor cell proliferation. Conversely the number of Alkaline Phosphatase (ALP) positive colonies (CFU-AP) in *Lpar1*ΔOb was higher than in CTRL (Fig. 2A-B). The monitoring of ALP activity by

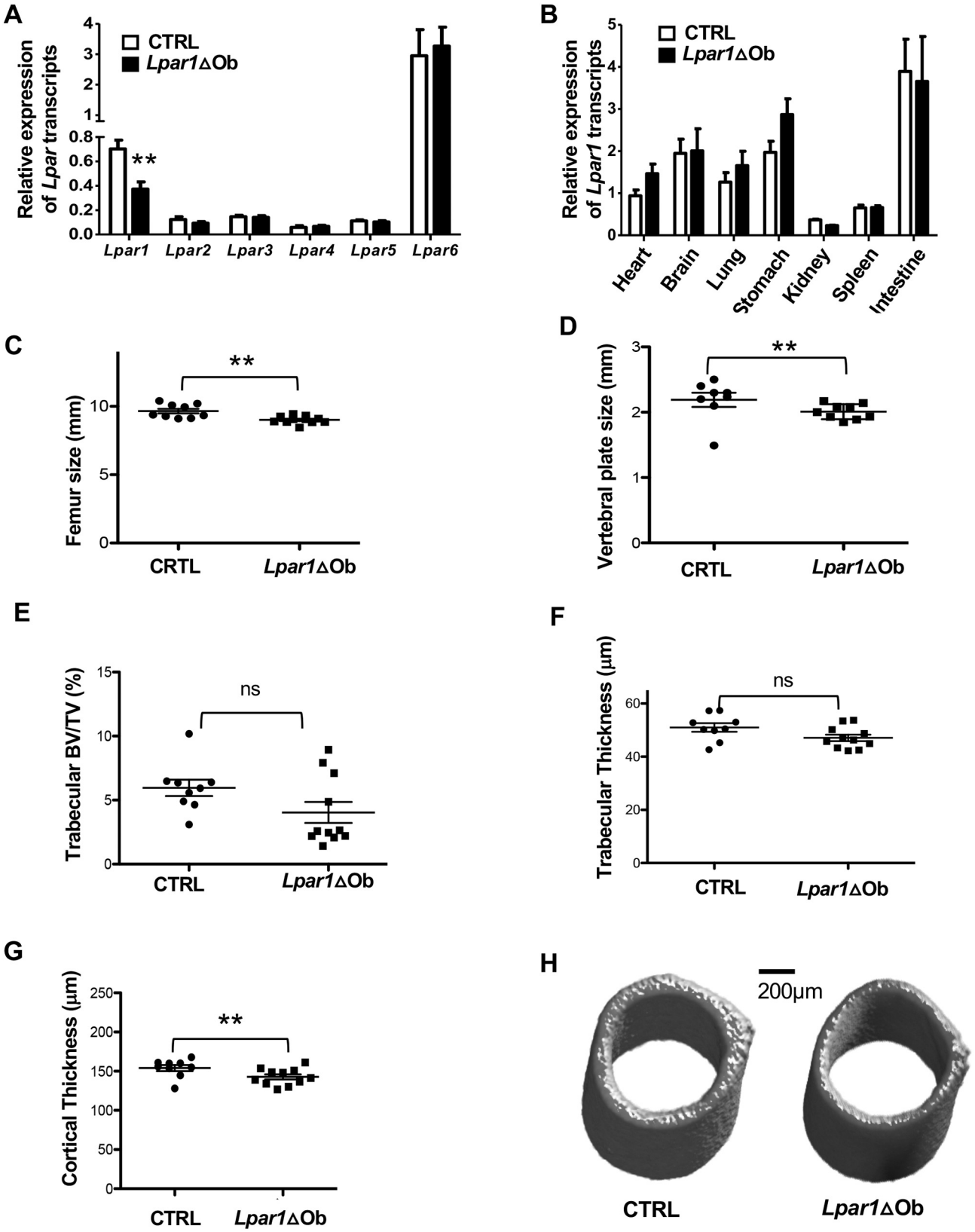

Fig. 1. Lpar1 selective deletion in osteoblasts affects bone morphometric parameters. A- Real-time expression of LPA receptor transcripts in bone, values are the mean ± SEM $^{**}p < 0{,}01$ assessed by ANOVA. B- Real-time expression of *Lpar1* transcript levels in various tissues and selective *Lpar1* deletion in osteoblasts. C– For mice analysis samples were respectively CTRL $n = 9$ and *Lpar1*△Ob $n = 11$ -femur and D-vertebra size values of 1 month old female mice from each genotype,** $p < 0{,}005$ assessed by Mann-Whitney test. D- Bar charts of trabecular bone mass quantification showing BV/TV values of CTRL and *Lpar1*△Ob mice from femur microcomputed tomography (µCT) analysis CTRL n = 9 and *Lpar1*△Ob = 11 assessed by Mann-Whitney test. *E*- Bar charts of femur cortical thickness values from CRTL and *Lpar1*△Ob mice $^{*}p < .05$ assessed by Mann-Whitney test. F- Representative 3D-µCT reconstruction images of midshaft femur cross section from CTRL and *Lpar1*△Ob mice.

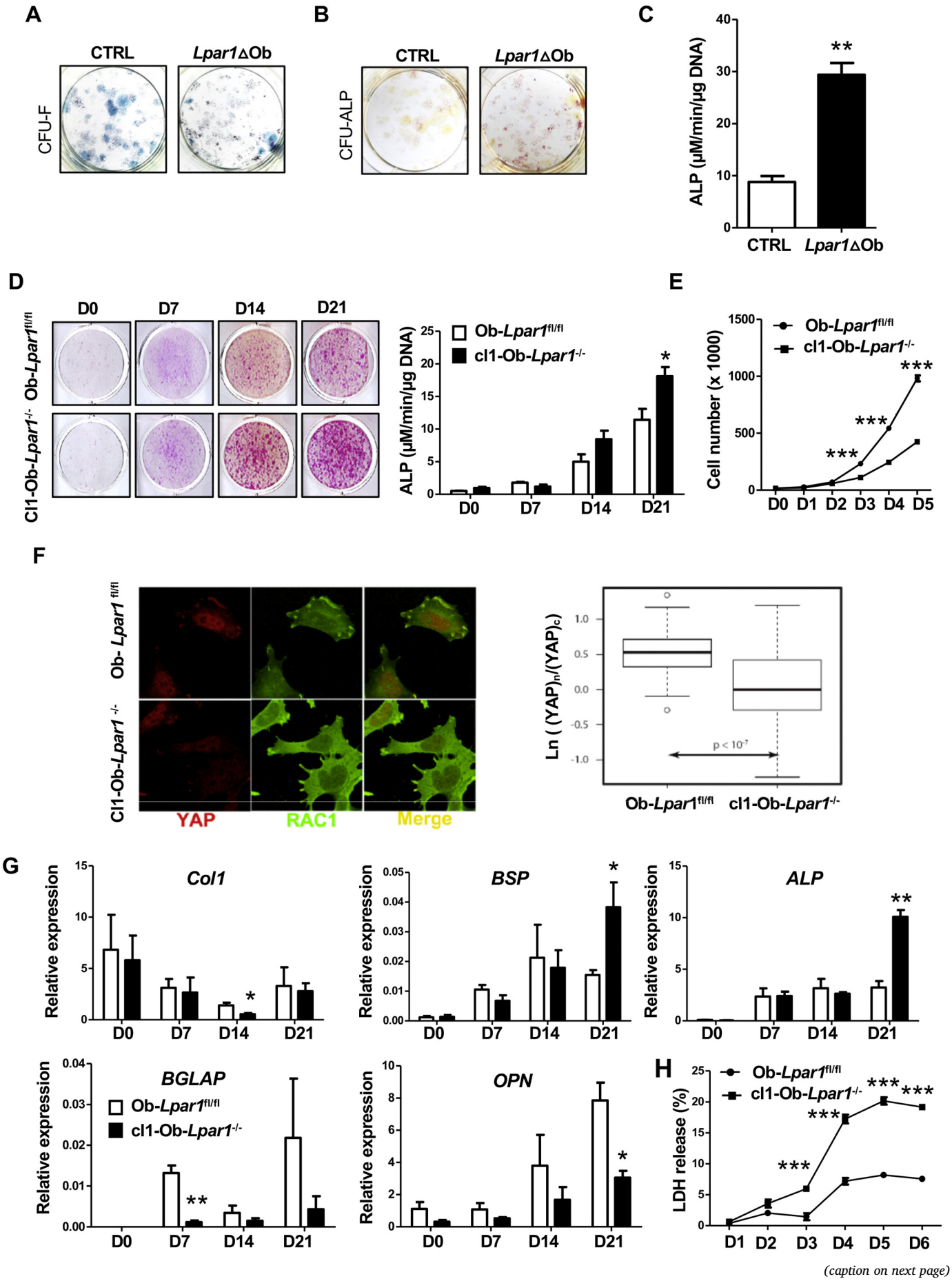

(caption on next page)

Fig. 2. *Lpar1*-deficient osteoblasts showed reduced proliferation, increased ALP activity and altered differentiation. Primary mouse BMSCs from 3 week old CTRL and *Lpar1*△Ob mice were cultured in osteogenic differentiation medium for 21 days and corresponding cells were (A) stained with methylene blue for total number of colony-forming-unit-fibroblasts (CFU-F) and B- stained for Alkaline Phosphatase (ALP) for total number of CFU-ALP. C– ALP dosage of CTRL and *Lpar1*△Ob D21 Ob. D- Preosteoblasts immortalized clones Cl1-Ob-*Lpar1*$^{-/-}$ and Ob-*Lpar1*$^{fl/fl}$ were plated at the same density, cultured in the non-osteogenic medium and at each time-point, cells were counted $n = 3$. ALP activity was analyzed by either staining of osteogenic culture or by colorimetric dosage at each time-point. E- Lpa1 deficiency induced ALP activity increase in early osteoblasts. *Cl1Ob-Lpar1*$^{-/-}$ and Ob-*Lpar1*$^{fl/fl}$ clones were cultured in the osteogenic medium for 21 days and ALP activity was analyzed by staining and colorimetric dosage at days 0,7,14 and 21, n = 3. values are the mean ± SEM *$p < .05$ assessed by Mann-Whitney test. F-Immunostaining of Yap (red) and Rac1 (green) on Cl1-Ob-*Lpar1*$^{-/-}$ and Ob-*Lpar1*$^{fl/fl}$ clones Scale bar statistical analysis of YAP nuclear to cytoplasmic ratio. Data are represented on a logarithmic scale. $n = 50$; statistical significance of differences was assessed by a two-tailed unpaired Student's *t*-test, and the box plot is representative of three independent experiments. G- Cl1-Ob-*Lpar1*$^{-/-}$ and Ob-*Lpar*1 $^{fl/fl}$ clones were cultured in the osteogenic medium. Real-time PCR showing relative expression levels of osteoblast differentiation markers; values are the mean ± SEM *p < .05,**$p < .01$ assessed by Mann-Whitney test. H– Cl1-Ob-*Lpar*1$^{-/-}$ and Ob-*Lpar1*$^{fl/fl}$ cells were plated at the same density for 6 days and fluorimetric LDH release assay was performed following serum starvation to assess cell viability, values are the mean ± SEM ***$p < .001$ assessed by Mann-Whitney test.

an enzymatic assay in *Lpar1*ΔOb osteoblasts confirmed the increased ALP expression over that of CTRL (Fig. 2 C). To facilitate the follow-up of *Lpar1*-depleted osteoblast cell differentiation *in vitro*, *Lpar1*$^{fl/fl}$ primary calvaria osteoblasts were immortalized and used as controls (Ob-*Lpar1*$^{fl/fl}$) or subsequently deleted for *Lpar1* by adenovirus infection driving Cre expression, generating *Lpar1* $^{-/-}$ osteoblasts (clone cl1-Ob-*Lpar1*$^{-/-}$).

Time sequential ALP staining of Ob -Lpar1 $^{fl/fl}$ and cl1-Ob-*Lpar1*$^{-/-}$osteogenic cultures showed an overall increase of ALP staining and activity significant at end point, but visible at day 7 suggesting a delayed differentiation (Fig. 2D). Proliferation curves showed a significantly proliferation defect at days 3, 4 and 5 for cl1-Ob-*Lpar1*$^{-/-}$ with respect to Ob-*Lpar1*$^{fl/fl}$ (Fig. 2E). In addition, cl1-Ob-*Lpar1*$^{-/-}$ displayed a significant decrease in cell viability compared to Ob -*Lpar1*$^{fl/fl}$ (Fig. 2H). These results, combined with the data obtained with *Lpar1*ΔOb derived from MSCs, highlight the importance of LPA_1 expression for tuning osteoblast proliferation *versus* cell differentiation.

YAP/TAZ activation is required for the expression of some LPA-induced genes and plays a critical role in cell proliferation in response to LPA [30]. YAP/TAZ is activated by $G\alpha_{12/13}$, $G\alpha_{i/O}$, $G\alpha_{q/11}$ that are also hallmark transducers of intracellular signals of LPA_1 activation [30]. YAP promotes osteogenesis by controlling cell proliferation in the Ob-cell lineage and suppressing adipogenesis [31]. Further studies have shown the crucial role of YAP expression and its rac1-dependent cellular localization in growth and proliferation pathways. Accordingly, Ob -*Lpar1* $^{fl/fl}$ and cl1-Ob-*Lpar1*$^{-/-}$ osteoblasts were examined by immunolabeling for their YAP and rac1 expression and cellular localization upon fibronectin adhesion (Fig. 2F). Ob-*Lpar1*$^{fl/fl}$ displayed YAP nuclear localization as well as accurate rac1 binding to focal adhesion structures, but conversely in cl1-Ob-*Lpar1*$^{-/-}$ osteoblasts, YAP and Rac1 were found to be diffused throughout the cytoplasm. Quantification of the YAP nuclear/cytoplasmic ratio showed a significantly decrease in cl1-Ob-*Lpar1*$^{-/-}$ *versus* Ob-*Lpar1* $^{fl/fl}$ ($n = 50$) indicating a strong mis-regulation of the YAP pathway. Overall, these results suggest that alteration of the LPA/LPA_1/YAP pathway may result in reduced survival of cells in the osteoblast lineage.

To further study the impact on differentiation of *Lpar1* deletion in osteoblasts, time course expression of major osteogenic markers was assessed (Fig. 2G). In cl1-Ob-*Lpar1*$^{-/-}$, ALP and BSP were found to be elevated at the end point of differentiation whereas Col1, Bglap and Opn were significantly decreased compared to *Lpar1*$^{fl/fl}$ osteoblasts. Overall, sequential osteogenic gene expression is disturbed when *Lpar1* is lacking in osteoblasts, suggesting a delay in osteoblast maturation. Cl1-Ob-*Lpar1*$^{-/-}$ cells revealed a remarkable decrease in cell viability compared to Ob-*Lpar1*$^{fl/fl}$ cells as judged by a significant increase in LDH release starting from D3 after starvation (Fig. 2H).

3.3. Hypomineralization phenotype of Lpar1ΔOb mice

We have shown that cl1-Ob-*Lpar1*$^{-/-}$ cells display up-regulated ALP transcript levels compared to *Lpar1*$^{fl/fl}$ osteoblasts during osteogenic differentiation. Because ALP is involved in matrix mineralization, we then monitored the ability of cl1-Ob-*Lpar1*$^{-/-}$ to mineralize the matrix *in vitro* using Alizarin Red staining. In comparison to *Lpar1*$^{fl/fl}$ osteoblasts Cl1-Ob-*Lpar1*$^{-/-}$ cells showed a strong delay in the time course to achieve bone matrix mineralization (Fig. 3A). This last result prompted us to investigate to what extent bone mineral properties are affected in *Lpar1*ΔOb mice with respect to CRTL mice. MicroCT analysis revealed that cortical femur bone mineral density (BMD) values from *Lpar1*ΔOb mice were significantly lower than those of CRTL mice (Fig. 3B) and suggested an hypomineralization in *Lpar1*ΔOb bones. Indeed, the degree of bone mineralization measured by X-ray microradiography analysis on tibia cortical sections confirmed a significant decrease in mineral content in *Lpar1*ΔOb *versus* CRTL long bones (Fig. 3C), further supported by a lower mineral/organic ratio quantified by FTIRM bone analysis (Fig. 3 D). Taken together, these data indicate that *Lpar1* deficiency in osteoblasts results in a defect of bone mineralization.

3.4. Bone cortical defect in Lpar1ΔOb mice

The hypomineralization and reduced cortical thickness observed on *Lpar1*ΔOb long bones suggest that *Lpar1* deficiency in osteoblastic cell lineage might could potentially deeply impact on cortical bone quality and structure. In order to examine this point, we analyzed cortical bone structure and cellular content. Cortical porosity of both femurs and tibias were assessed by two different technical approaches. Cortical porosity was first assessed by μCT analysis at the midshaft of the femurs. *Lpar1*ΔOb bones revealed a significantly higher cortical porosity than those of CTRL (Fig. 4A). Consistently, microradiography digitized image analysis showed that *Lpar1*ΔOb tibia cortical porosity was significantly higher than *Lpar1*$^{fl/f}$ tibia transverse sections, which resulted in an increased number of pores in the range of osteocyte lacunaes (Fig. 4B).

The cellular content of compact bone is mainly composed of osteocytes (90%), which are fully differentiated osteoblasts embedded in the bone matrix [32]. Consequently, specific *Lpar1* deletion in osteoblast could potentially affect the osteocyte phenotype. To provide more insights into the cortical bone defect in *Lpar1*ΔOb mice, osteocyte distribution and viability were assessed by histological analyses of cortical bone performed on midshaft femur sections. Similar numbers of osteocytes per mm^2 were found in both genotypes whereas the mean size of osteocyte lacunae areas appeared to be larger in the bone of *Lpar1*ΔOb mice than CTRL mice, confirming previous X-ray microradiography digitized imaging results (Fig. 4C). These results suggest altered osteocyte behavior in *Lpar1*ΔOb mice. This hypothesis was further supported by histological analyses of cortical bone sections stained for TUNEL and cleaved Caspase-3 assays showing a significant increase in the number of TUNEL-positive (Fig. 4D) and activated Caspase 3-positive cells/mm^2 (Fig. 4E) in *Lpar1*ΔOb cortical bone compared to CTRL. These results indicate for the first time that altered LPA_1 signaling in osteoblastic cell lineage promotes osteocyte apoptosis *in vivo*.

Osteocytes are endocrine cells that orchestrate bone remodeling and

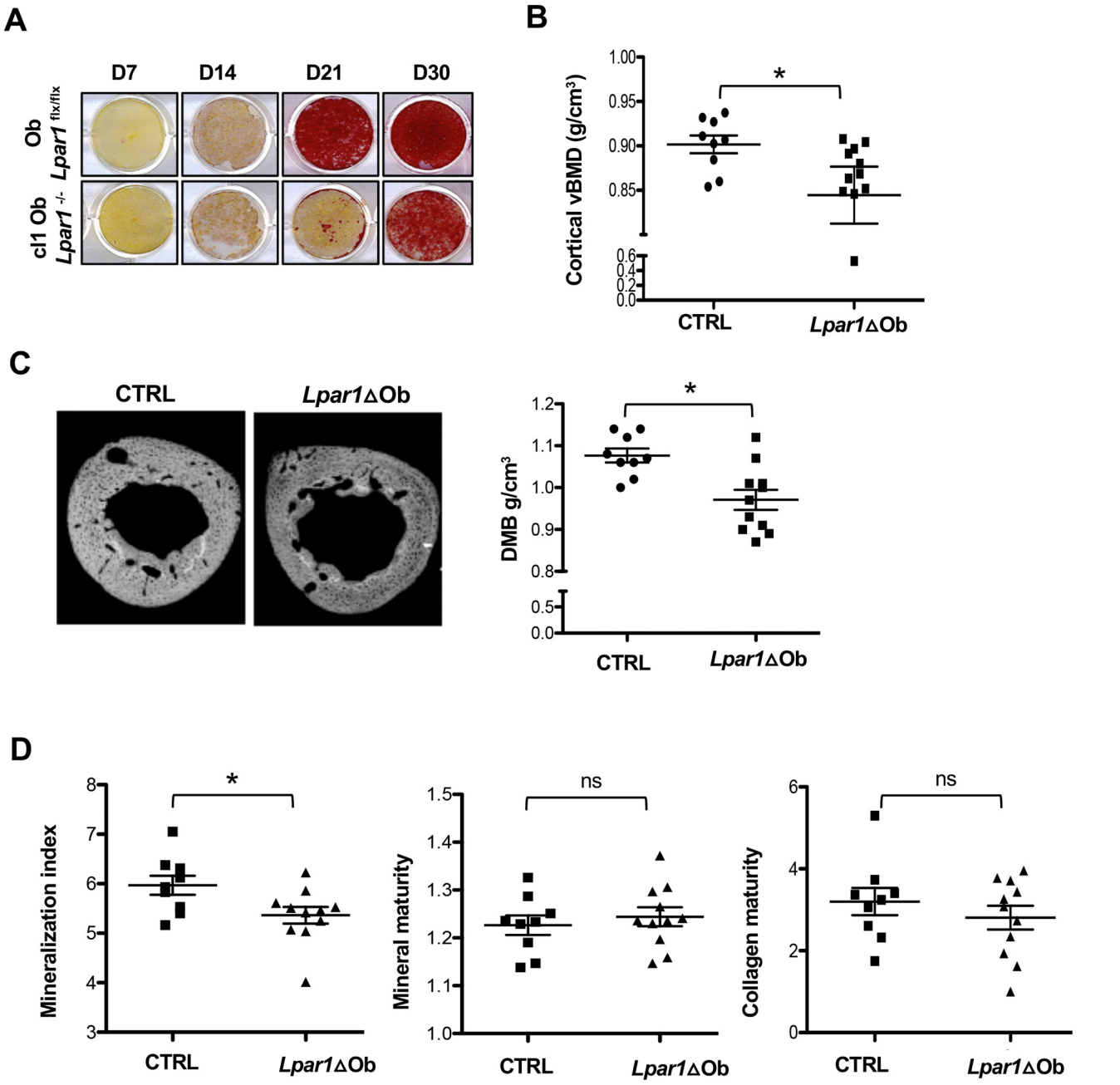

Fig. 3. Defective bone mineralization in *Lpar1*△Ob mice.
A- Mineralization was analyzed by Alizarin Red staining at days 7,14,21 and 30 of culture. B- Cortical volumetric bone mineral density (vBMD) was measured from digitally extracted 3D bone cortical volumes of CTRL and *Lpar1*△Ob femur *$p < .05$, assessed by Mann-Whitney test. C- Digitized microradiography images (upper panel) and corresponding DMB (degree of bone mineralization) of cortical tibia section from CTRL and *Lpar1* △ mice (lower panel) values are the mean ± SEM *$p < .05$, assessed by Mann-Whitney test. D- Fournier Transformed Infra Red Microscopy (FTIRM) analysis showing mineral index, mineral and collagen maturity of CTRL and *Lpar1* △Ob mice tibia, values are the mean ± SEM *$p < .05$, assessed by Mann-Whitney test.

calcium homeostasis through secreted factors such as sclerostin and FGF-23 [32]. To better characterize the osteocyte phenotype in *Lpar1*ΔOb mice, we performed real-time PCR of osteocyte markers in bone explants (Fig. 4E). E11 (podoplanin), an actin fiber bundle connector which is involved in dendrite formation [33] and expressed mainly in embedding osteoblasts and mineralizing osteocytes was strongly reduced in *Lpar1*ΔOb bone explants (Fig. 4E). Dkk1 (Dikkopf-related -protein-1) a wnt pathway antagonist [34] and Dmp1 (Dentin Matrix Protein1) were also significantly down-regulated in *Lpar1*ΔOb bone explants compared to CTR. In contrast, the level of transcripts corresponding to matrix proteins, PHEX and MEPE, as well as Connexin 43, were not significantly altered in CTRL bone explants. Sost (sclerostin transcript) which is expressed in mature osteocytes and is instrumental for osteocyte-mediated control of bone remodeling, was strikingly decreased in *Lpar1*ΔOb bone explants. Taken together, these results indicate that *Lpar1* deficiency in osteoblasts results in a defect of osteocyte homeostasis.

3.5. Osteocyte dendrite network is affected by osteoblast Lpar1 deficiency

Osteocytes are mechanosensors and mechanotransducers responsible for the adaptation of bone to internal and external stress. They form a dense highly connected dendritic network that extends from the cell body through bone canaliculae, allowing communications

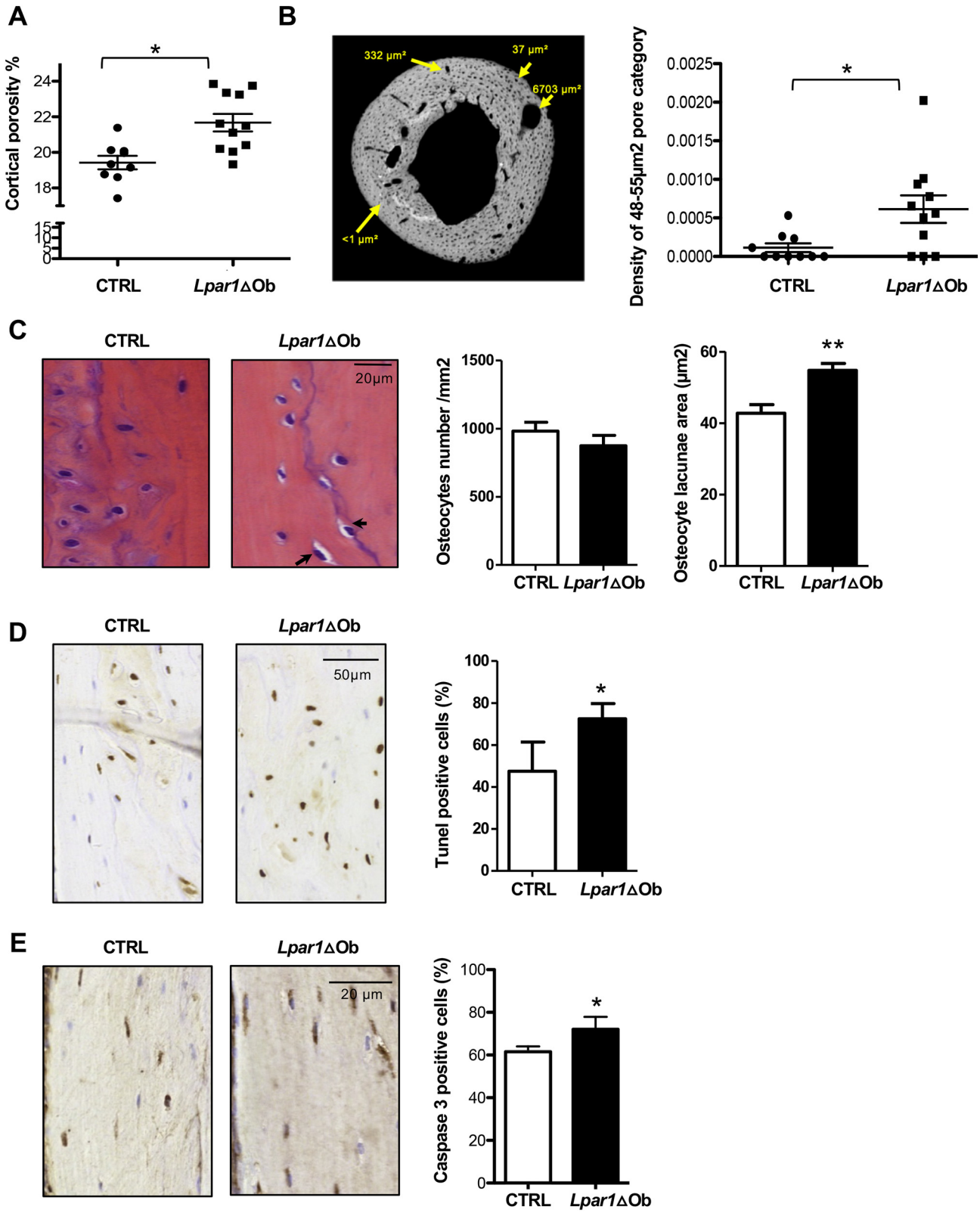

Fig. 4. – *Lpar1* selective deletion in osteoblasts impacts osteocytes and increases cortical porosity. A - Percentage of bone cortical porosity was evaluated from digitally extracted 3D µCT bone cortical volume femur analysis of CRTL $n = 8$ and *Lpar1*△Ob $n = 11$ $^{*}p < .05$, assessed by Mann-Whitney test. B- Tibia cortical porosity: pore density over the total cortical surface was measured by quantitative microradiography, values from 70 to 79 µm^2 were considered for each genotype; values are ± SEM $^{*}p < .05$, assessed by Mann-Whitney test. C- Representative hematoxilin staining of femur cortical sections of CRTL and *Lpar1*△Ob from 3 week old mice. Arrows indicate enlarged lacunae around osteocytes in *Lpar1*△Ob, the number of osteocytes/mm^2 were counted and numbers reported in the corresponding bar chart. D-E Representative TUNEL (D) and cleaved Caspase-3 (E) staining of cortical section of Crtl and *Lpar1*△Ob femur from 3 week old mice and corresponding quantitative bar charts; values are the mean ± SEM $^{*}p < .05$, assessed by Mann-Whitney test. F- Real-time PCR of osteocyte markers expression in flushed long bones of both genotype values are the mean ± SEM $^{*}p < .05$, and $^{**}p < 0{,}01$ assessed by Mann-Whitney test.

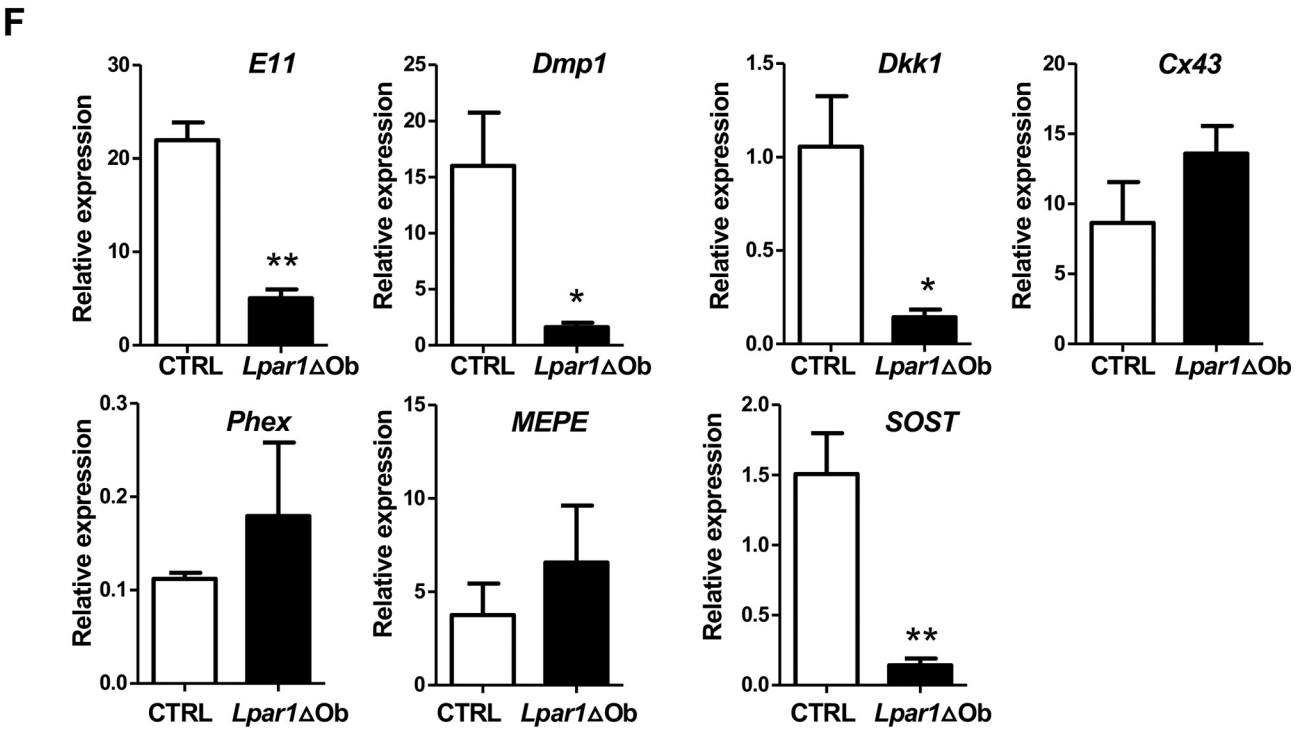

Fig. 4. (*continued*)

and interactions with the vasculature and bone endosteum [35]. Fibroblastic growth factor 2 (FGF2) is known to induce dendrite extension from osteoblasts *in vitro* [36]. We therefore decided to explore the osteocyte dendrite pattern in cl1-Ob-*Lpar1*$^{-/-}$ cells through labeled actin filament under FGF2 treatment. As anticipated, FGF2 promoted filament extensions in *Lpar1*$^{fl/fl}$ cells but almost no dendrite extensions in cl1-Ob-*Lpar1*$^{-/-}$ cell culture (Fig. 5A). Similar experiments were performed on primary osteoblasts from CRTL and *Lpar1*ΔOb mice. In these conditions FGF2 induced the formation of a dense dendrite network in CTRL cells, that was absent in *Lpar1*ΔOb cells (Fig. 5B). In agreement with these findings FGF2 failed to upregulate the expression of the E11osteocyte marker, both at the transcriptional (Fig. 5C) and protein (Fig. 5D) levels in cl1-Ob-*Lpar1*$^{-/-}$ cells compared to Ob-*Lpar1*$^{fl/fl}$ cells. Confocal analyses showed that osteocyte dendrite numbers/mm^3 was significantly decreased in the cortical bone of *Lpar1*ΔOb mice compared to CTRL mice (Fig. 5E). Altogether, these results revealed a major role for LPA_1 in dendrite formation and osteocyte maturation.

4. Conclusions

LPA is a lipid mediator that controls bone homeostasis by exerting complex effects on all types of bone cells as well as bone marrow and vascular cells [8]. Previous studies from our laboratories and others have shown that LPA through its receptor LPA_1 promotes both bone formation and bone resorption [9,10]. As a consequence, despite their extent, *in vivo* analyses of the *Lpar1*$^{-/-}$ mouse bone phenotype failed to unravel the specific role of LPA_1 in bone homeostasis. In this study, we have investigated the specific role of the LPA/LPA_1 pathway in bone-forming cells *in vivo* by generating *Lpar1*ΔOb mice by conditional deletion of *Lpar1* in osteoblastic cell lineage.

*Lpar1*ΔOb mice showed a milder deterioration of the bone microstructure than *Lpar1*$^{-/-}$ mice that exhibit strong osteoporosis [15]. In addition, *Lpar1*$^{-/-}$ mice reveal a strong alteration in growth that is not observed in *Lpar1*ΔOb mice at the same age although these mice had a significant moderate reduction in size of the femurs and L5 vertebrae. The differences between these two genetically modified mouse lines may have multiple causes as LPA_1 is the most ubiquitous of all LPA receptors. *Lpar1*$^{-/-}$ mice have major defects in the nervous and adipose systems and in metabolic functions controlling glucose tolerance, which may significantly impair the mouse growth [14–16] but which should not be affected in *Lpar1*ΔOb mice. Cranio-facial, sternal and costal abnormalities are characteristics of *Lpar1*$^{-/-}$ animal phenotype which are due to impaired chondrocyte activity and endochondral ossification [9]. Unexpectedly, these characteristics were not found in *Lpar1*ΔOb mice although Osx-cre:GFP expression is also detected in hypertrophic chondrocyte zone at the growth plate [37]. Nevertheless, the absence of morphogenic defects in *Lpar1*ΔOb mice might reinforce previous hypothesis claiming the essential role of LPA_1 in chondrocytes [9,13]. Nevertheless, *Lpar1*$^{-/-}$ and *Lpar1*ΔOb mice revealed a series of similar bone defects such as decrease in cortical thickness and mineralization, which are associated with decreased osteogenesis of bone marrow mesenchymal cells and expression of bone markers (Col1, Bglap) compared to WT and control animals, respectively. As a new observation, our results in *Lpar1*ΔOb mice highlighted the essential role of LPA_1 in osteocytogenesis and on organization of the osteocyte dendrite network.

Osteoblasts derived from *Lpar1*ΔOb bone marrow mesenchymal cells displayed a lower ability to generate colony-forming-units (both in size and number) *in vitro* suggesting a cell proliferation defect in early progenitors. This hypothesis agrees with the proliferative and pro-survival action of LPA *via* LPA_1 in murine and human bone marrow mesenchymal cells [8,38]. In addition, immortalized cl1-Ob-*Lpar1*$^{-/-}$ osteoblasts revealed a significant decrease in cell survival associated with a significant decrease in the YAP nuclear/cytoplasmic ratio. YAP/TAZ activation is required for the expression of some LPA-induced genes and plays a critical role in cell proliferation in response to LPA [30]. These results suggest that deregulation of the YAP pathway may be a major cause of reduced cell survival of osteoblastic cells deficient in LPA_1. Deletion of YAP or its co-activator TAZ from osteoblast-lineage cells causes lethality in mice due to skeletal fragility [39]. Recently, the co-deletion of YAP/TAZ was shown to increase osteocyte apoptosis and to impair osteocyte perilacunar/canalicular remodeling by reducing canalicular network density, length, and branching [40]. *Lpar1*ΔOb

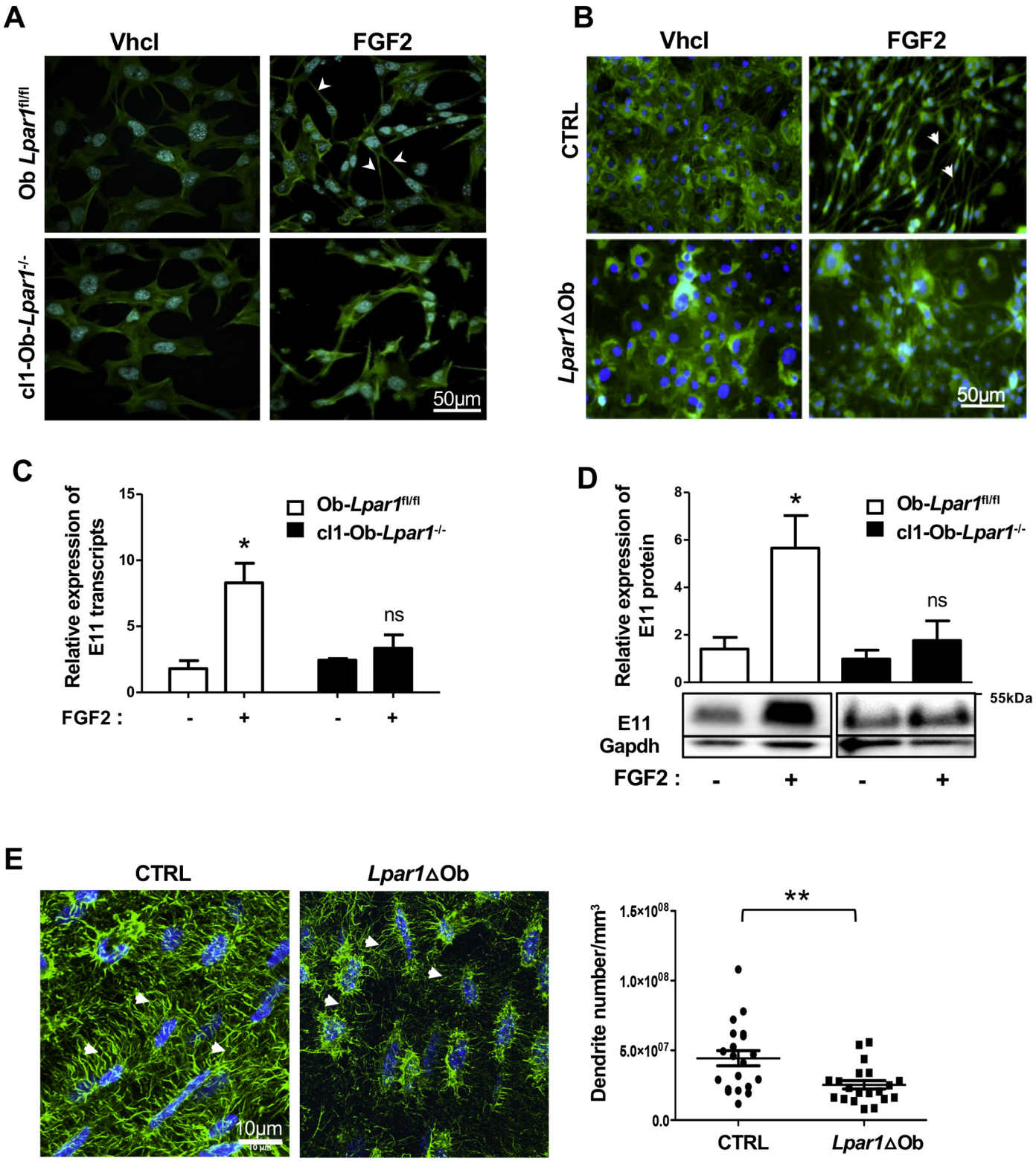

Fig. 5. *Lpar1* deletion impairs osteocyte dendrite formation

A- Representative micrographs of immortalized clones Cl1-Ob-*Lpar1*$^{-/-}$ and B- Ob-*Lpar1*$^{fl/fl}$ primary CTRL and *Lpar1*△Ob osteoblasts treated with FGF2 (10 ng/ml) for 3 days and stained for actin filament visualization (Alexa Fluor 488 Phalloidin, arrowheads) and for nuclei (Hoechst, bleu). C- Real-time PCR for E11 in Cl1-Ob-*Lpar1*$^{-/-}$ and Ob-*Lpar1*$^{fl/fl}$ clones after FGF2 (10 ng/ml) challenge for 4 h compared to vehicle. D- Representative Western blot and quantification showing E11 protein expression in immortalized clones Cl1-Ob-Lpar1 −/− and Ob-Lpar1fl/fl after 24 h challenge, where (+) is FGF2 treated cells, and (−) is vehicle treated control. Results were normalized by the GAPDH protein for loading control. E- 3D-Deconvoluted Z stack images of cortical bone, were analyzed for quantification of dendrites/mm^3 (arrowheads) $n = 3$ mice per genotype and 2 zones of 3 sections/mice were measured; values are the mean ± SEM $^*p < .05$, and $^{**}p < 0{,}01$ assessed by Mann-Whitney test.

mouse osteocytes exhibited *in vivo* similar profound increase in apoptosis rate and impaired canalicular network density suggesting that LPA/LPA_1 axis may contribute to YAP/TAZ osteocytogenesis activity. Other types of LPA receptors expressed in osteoblasts are also known to activate YAP/TAZ especially in different cellular contexts such as LPA_4 through $G\alpha_{12/13}$ that promotes developmental angiogenesis [41]. As opposed to the osteoporotic phenotype of *Lpar1*$^{-/-}$ mice, *Lpar4*$^{-/-}$ mice exhibit an osteopetrotic bone phenotype [42]. Both LPA receptors activate $G\alpha_{12/13}$ [5]. In this respect inactivation of one of the receptors should be compensated, at least partially, by expression of the other. This was not observed in clone cl1-Ob-*Lpar1*$^{-/-}$ osteoblasts. However, the shift from a $G\alpha_{i/O}$ pathway induced by LPA_1 to a $G\alpha_S$ pathway induced by LPA_4 in osteoblasts has been proposed to contribute to the opposing bone phenotypes of global knockout animals [43]. The $G\alpha_S$ signaling pathway activates Lats1/2 which blocks downstream YAP/TAZ activation [30]. Our data therefore support the notion of a prevalence of the LPA/LPA_4/$G\alpha_S$ pathway in osteoblasts in the absence of LPA_1 expression.

Lpar1 deficiency in osteoblasts leads to an alteration in osteogenic maturation reflected by increased expression of BSP, ALP transcription and activity. Poor mineralization is also associated with high levels of mRNA and ALP activity in osteoblasts of hypophosphatemic (Hyp) mice due to loss of Phex function [44], but as such, increased ALP cannot explain the reduction in mineralization. Therefore, the primary defect responsible for osteoblast hypomineralization phenotype in *Lpar1*ΔOb mice is not fully understood. Collagen fibril deposition, assembly and maturation are essential for initiation of mineralization [45,46]. Intriguingly, reduced expression of Col I was also observed in *Lpar1*ΔOb mouse osteoblasts and in clone cl1-Ob-*Lpar1*$^{-/-}$ osteoblasts that may contribute to insufficient mineralization. Moreover, the expression of matrix proteins Col I, BGLAP and OPN in cl1-Ob-*Lpar1*$^{-/-}$ cells and Dmp1 in *Lpar1*ΔOb bone explants are significantly down-regulated. Interestingly, the temporal shift of increase in ALP and BSP transcripts and decay in the level of bone matrix proteins (Col I, OPN, Dmp1) is found in aging and senescent osteoblasts [47,48]. Our data suggest that *Lpar1*-deficient osteoblasts are prematurely engaged in an aging program. Aging has a remarkable influence on bone quality, as shown by a decrease in cortical thickness associated with an increase in cortical porosity which is characteristic of the bone quality during aging in women [49]. MicroCT, microradiography and histological analyses of the long bones of *Lpar1*ΔOb mice reveal a significant reduction in cortical thickness and an increase in cortical porosity, confirming the idea that *Lpar1* deficiency in osteoblasts may promote premature bone aging.

Unbalanced expression of bone matrix proteins in osteoblasts could lead to poor quality of bone mineralization [50]. Indeed, cl1-Ob-*Lpar1*$^{-/-}$ cells cultured under osteogenic conditions showed diminution of Alizarin Red staining indicating alteration of cell mineralization capacity *in vitro*. This defect is likely to explain several bone characteristics of *Lpar1*ΔOb mice that displayed a low cortical bone mineral density assessed by μCT, a low degree of mineralization assessed by microradiography and a significant decrease in the mineral index/organic ratio determined by FTIRM analysis. Overall, *Lpar1*ΔOb mice presented a marked hypo-mineralization phenotype.

Besides poor mineralization impairing bone quality, hypo-mineralization has also been shown to affect osteocyte perilacunal and canalicular remodeling as detected in the Hyp-mouse model of X-linked hypophosphatemia [51]. Osteocytes are the most abundant cells in bone representing > 90% of total bone cells [52].These cells correspond to the terminal stage of osteoblast differentiation that eventually become embedded into their own bone matrix [52]. Osteocytes are mechanosensor cells that inhibit bone formation under steady state conditions [32]. In the context of hypo-mineralization observed in *Lpar1*ΔOb mice, histological sections of *Lpar1*ΔOb cortical bone display augmented osteocyte apoptosis and larger lacunar cavities. In agreement with previous findings showing that the LPA/LPA_1 axis is important for osteoblast cell lineage survival [53,54] our study suggests that the LPA/LPA_1 axis could also potentially impact on osteocyte survival through bone mineralization. Osteocyte markers such as Dmp1, and the wnt pathway inhibitors Dkk1 and Sost are dcreased in bone explants of *Lpar1*ΔOb mice. This result was rather unexpected because *Lpar1*ΔOb mice exhibited only a mild bone loss phenotype with a decrease in cortical bone thickness, whereas Sost-deficient mice have a strong osteopetrotic phenotype [55]. Moreover, targeting SOST with romosozumab has recently been validated as a novel therapy for osteoporosis [56]. Nevertheless, our data agree with recent reports showing that despite a drastic decrease of osteocytic markers including Sost, *Ppargc1a/b* conditional knockout mice osteoblasts and osteocytes exhibit an osteopenic bone phenotype [57] indicating that miss-egulation of multi-gene programs both in osteoblasts and osteocytes, such as in *Ppargc1a/b* conditional knockout mice or *Lpar1*ΔOb mice, may affect wnt inhibitor production but without promoting bone formation.

Nonetheless, another osteocyte marker E11 or podoplanin is downregulated in bone explants from *Lpar1*ΔOb mice. E11 is an important autocrine osteocyte factor, which starts to be expressed at the time the osteoblast is embedded in the organic matrix. E11 expression is later required for the process of dendritic projection and branching during osteocyte differentiation [35]. LPA has been shown to induce dendrite outgrowth in MLO-Y4 osteocytic cells that is inhibited by Ki16425, a non-selective inhibitor of LPA_1/LPA_3 receptors and pertussis toxin which inhibits the $G\alpha_i$ pathway [11]. In contrast to CTRL osteoblasts, E11-dependent induction of dendrite extensions by FGF2 is abrogated in *Lpar1*ΔOb and cl1-Ob-*Lpar1*$^{-/-}$ osteoblasts. Experiments carried out with MLO-Y4 cells showed that LPA induced-dendritogenesis is a membrane- and cytoskeleton-driven process with actin dynamics playing a critical role [58]. Our results suggest that LPA_1 triggers actin cytoskeleton remodeling that promotes membrane extensions through E11 activation during osteocyte differentiation.

In conclusion, our study shows tor the first time that expression of LPA_1 in osteoblastic cell lineage controls bone mineralization and osteocyte specification. Our study raises caution about long term inhibition of LPA_1 activation that could potentially favor premature bone aging.

Credit author statement

Candide A. Alioli and Léa Demesmay: animal experimentation, cell biology and histology, Sara Laurencin-Dalacieux: design experiments, Nicolas Beton: genotyping and QRT-PCR, Delphine Farlay and Helene Follet: FTIRM and bone histology, Amri Saber: QRT-PCR, François Duboeuf: microCT, Jerold Chun and Richard Rivera: animal generation, characterization, reviewing and editing, Daniel Bouvard: Cell immortalization, YAP/Rac1 experiments, reviewing and editing, Irma Machuca- Gayet: Confocal imaging, writing and editing, Jean-Pierre Salles: Reviewing and editing, Isabelle Gennero and Olivier Peyruchaud: Oversight of the project, writing- reviewing and editing.

Funding sources

This work was supported by grants from the Institut National de la Santé Et de la Recherche Médicale, the Université Claude Bernard Lyon 1, the Agence Nationale de la Recherche (Grant LYSBONE No. ANR-15-CE14-0010), the Région d'Occitanie (grant Rbio N°15065647), Ipsen Pharma France, Lilly France and Pfizer France.

Declaration of competing interest

The authors declare that they have no known competing financial interests or personal relationships that could have appeared to influence the work reported in this paper.

Acknowledgements

The authors would like to thank Rachel Balouzat and the staff members of the animal care facility US006/CREFRE (Toulouse, France) for technical assistance in animal experiments. The authors would like to thank the technical assistance of Florence Capilla and the staff members of the histology core facility in CPTP (US006 CREFRE) and the Odontology technical platform PLTRO in Toulouse and Denis Ressnikoff from the CIQLE plateform (Lyon, France) for technical assistance on imaging.

References

[1] K. Burton, N. Kendall, Musculoskeletal Disorders, the BMJ, (2014), https://doi.org/10.1136/bmj.g1076.
[2] S.J. Duffield, B.M. Ellis, N. Goodson, K. Walker-Bone, P.G. Conaghan, T. Margham, T. Loftis, The contribution of musculoskeletal disorders in multimorbidity: implications for practice and policy, Best Pract. Res. Clin. Rheumatol. (2017), https://doi.org/10.1016/j.berh.2017.09.004.
[3] L.J. Raggatt, N.C. Partridge, Cellular and Molecular Mechanisms of Bone Remodeling, The J. Biol, Chem, 2010, https://doi.org/10.1074/jbc.R109.041087.
[4] A.J. Houben, W.H. Moolenaar, Autotaxin and LPA Receptor Signaling in Cancer, Cancer Metastasis Rev, (2011), https://doi.org/10.1007/s10555-011-9319-7.
[5] Y.C. Yung, N.C. Stoddard, J. Chun, LPA receptor signaling: pharmacology, physiology, and pathophysiology, J. Lipid Res. (2014), https://doi.org/10.1194/jlr.R046458.
[6] M. David, E. Wannecq, F. Descotes, S. Jansen, B. Deux, J. Ribeiro, C.M. Serre, S. Gres, N. Bendriss-Vermare, M. Bollen, S. Saez, J. Aoki, J.S. Saulnier-Blache, P. Clezardin, O. Peyruchaud, Cancer Cell Expression of Autotaxin Controls Bone Metastasis Formation in Mouse through Lysophosphatidic Acid-Dependent Activation of Osteoclasts, PloS One, (2010), https://doi.org/10.1371/journal.pone.0009741.
[7] A. Boucharaba, C.-M. Serre, S. Gres, J.S. Saulnier-Blache, J.-C. Bordet, J. Guglielmi, P. Clezardin, O. Peyruchaud, Platelet-derived lysophosphatidic acid supports the progression of osteolytic bone metastases in breast cancer, J. Clin. Invest. (2004), https://doi.org/10.1172/JCI22123.
[8] X. Wu, Y. Ma, N. Su, J. Shen, H. Zhang, H. Wang, Lysophosphatidic Acid: Its Role in Bone Cell Biology and Potential for Use in Bone Regeneration, Prostaglandins Other Lipid Mediat, (2019), https://doi.org/10.1016/j.prostaglandins.2019.106335.
[9] I. Gennero, S. Laurencin-Dalicieux, F. Conte-Auriol, F. Briand-Mesange, D. Laurencin, J. Rue, N. Beton, N. Malet, M. Mus, A. Tokumura, P. Bourin, L. Vico, G. Brunel, R.O. Oreffo, J. Chun, J.P. Salles, Absence of the Lysophosphatidic Acid Receptor LPA1 Results in Abnormal Bone Development and Decreased Bone Mass, Bone, (2011), https://doi.org/10.1016/j.bone.2011.04.018.
[10] M. David, I. Machuca-Gayet, J. Kikuta, P. Ottewell, F. Mima, R. Leblanc, E. Bonnelye, J. Ribeiro, I. Holen, R.L. Vales, P. Jurdic, J. Chun, P. Clezardin, M. Ishii, O. Peyruchaud, Lysophosphatidic acid receptor type 1 (LPA1) plays a functional role in osteoclast differentiation and Bone Resorption activity, J. Biol. Chem. (2014), https://doi.org/10.1074/jbc.M113.533232.
[11] S.A. Karagiosis, N.J. Karin, Lysophosphatidic acid induces osteocyte dendrite outgrowth, Biochem. Biophys. Res. Commun. (2007), https://doi.org/10.1016/j.bbrc.2007.03.121.
[12] S. An, T. Bleu, O.G. Hallmark, E.J. Goetzl, Characterization of a novel subtype of human G protein-coupled receptor for lysophosphatidic acid, J. Biol. Chem. (1998), https://doi.org/10.1074/jbc.273.14.7906.
[13] T. Nishioka, N. Arima, K. Kano, K. Hama, E. Itai, H. Yukiura, R. Kise, A. Inoue, S.H. Kim, L. Solnica-Krezel, W.H. Moolenaar, J. Chun, J. Aoki, ATX-LPA1 axis contributes to proliferation of chondrocytes by regulating fibronectin assembly leading to proper cartilage formation, Sci. Rep. (2016), https://doi.org/10.1038/srep23433.
[14] S.M. Harrison, C. Reavill, G. Brown, J.T. Brown, J.E. Cluderay, B. Crook, C.H. Davies, L.A. Dawson, E. Grau, C. Heidbreder, P. Hemmati, G. Hervieu, A. Howarth, Z.A. Hughes, A.J. Hunter, J. Latcham, S. Pickering, P. Pugh, D.C. Rogers, C.S. Shilliam, P.R. Maycox, LPA1 receptor-deficient mice have phenotypic changes observed in psychiatric disease, Mol. Cell. Neurosci. (2003), https://doi.org/10.1016/j.mcn.2003.09.001.
[15] J.J.A. Contos, N. Fukushima, J.A. Weiner, D. Kaushal, J. Chun, Requirement for the lpA1 Lysophosphatidic Acid Receptor Gene in Normal Suckling Behavior, PNAS, (2000), https://doi.org/10.1073/pnas.97.24.13384.
[16] R. Dusaulcy, D. Daviaud, J.P. Pradere, S. Gres, P. Valet, J.S. Saulnier-Blache, Altered food consumption in mice lacking lysophosphatidic acid receptor-1, J. Physiol. Biochem. (2009), https://doi.org/10.1007/BF03185929.
[17] G. Karsenty, Convergence between Bone and Energy Homeostases: Leptin Regulation of Bone Mass, Cell Metab, (2006), https://doi.org/10.1016/j.cmet.2006.10.008.
[18] R.R. Rivera, M.-E. Lin, E.C. Bornhop, J. Chun, Conditional Lpar1 gene targeting identifies cell types mediating neuropathic pain, bioRxiv (2020), https://doi.org/10.1101/2020.02.02.931212 2020.2002.2002.931212.
[19] S.J. Rodda, A.P. McMahon, Distinct Roles for Hedgehog and Canonical Wnt Signaling in Specification, Differentiation and Maintenance of Osteoblast Progenitors, Development, (2006), https://doi.org/10.1242/dev.02480.
[20] F. Montagner, V. Kaftandjian, D. Farlay, D. Brau, G. Boivin, H. Follet, Validation of a Novel Microradiography Device for Characterization of Bone Mineralization, J. Xray Sci, Technol, 2015, https://doi.org/10.3233/xst-150481.
[21] D. Farlay, M.E. Duclos, E. Gineyts, C. Bertholon, S. Viguet-Carrin, J. Nallala, G.D. Sockalingum, D. Bertrand, T. Roger, D.J. Hartmann, R. Chapurlat, G. Boivin, The Ratio 1660/1690 Cm(−1) Measured by Infrared Microspectroscopy Is Not Specific of Enzymatic Collagen Cross-Links in Bone Tissue, PloS One, (2011), https://doi.org/10.1371/journal.pone.0028736.
[22] D. Farlay, G. Panczer, C. Rey, P.D. Delmas, G. Boivin, Mineral maturity and crystallinity index are distinct characteristics of bone mineral, J. Bone Miner. Metab. (2010), https://doi.org/10.1007/s00774-009-0146-7.
[23] M. Gardegaront, D. Farlay, O. Peyruchaud, H. Follet, Automation of the Peak Fitting Method in Bone FTIR Microspectroscopy Spectrum Analysis: Human and Mice Bone Study, Journal of Spectrometry (2018), https://doi.org/10.1155/2018/4131029.
[24] E.P. Paschalis, E. DiCarlo, F. Betts, P. Sherman, R. Mendelsohn, A.L. Boskey, FTIR microspectroscopic analysis of human osteonal bone, Calcif. Tissue Int. (1996), https://doi.org/10.1007/bf00369214.
[25] H. Sabra, M. Brunner, V. Mandati, B. Wehrle-Haller, D. Lallemand, A.S. Ribba, G. Chevalier, P. Guardiola, M.R. Block, D. Bouvard, beta1 integrin-dependent Rac/group I PAK signaling mediates YAP activation of Yes-associated protein 1 (YAP1) via NF2/merlin, J. Biol. Chem. (2017), https://doi.org/10.1074/jbc.M117.808063.
[26] R.O. Oreffo, S. Romberg, A.S. Virdi, C.J. Joyner, S. Berven, J.T. Triffitt, Effects of interferon alpha on human osteoprogenitor cell growth and differentiation in vitro, J. Cell. Biochem. (1999), https://doi.org/10.1002/(sici)1097-4644(19990901)74:3<372::aid-jcb6>3.3.co;2-8.
[27] A.D. Bakker, J. Klein-Nulend, Osteoblast isolation from murine calvaria and long bones, Methods Mol. Biol. (2012), https://doi.org/10.1007/978-1-61779-415-5_2.
[28] J.Y. Li, M. Yu, A.M. Tyagi, C. Vaccaro, E. Hsu, J. Adams, T. Bellido, M.N. Weitzmann, R. Pacifici, IL-17 Receptor Signaling in Osteoblasts/Osteocytes Mediates PTH-Induced Bone Loss and Enhances Osteocytic RANKL Production, J. Bone. Miner, Res, 2019, https://doi.org/10.1002/jbmr.3600.
[29] M. Brunner, A. Millon-Fremillon, G. Chevalier, I.A. Nakchbandi, D. Mosher, M.R. Block, C. Albiges-Rizo, D. Bouvard, Osteoblast mineralization requires beta1 integrin/ICAP-1-dependent fibronectin deposition, J. Cell Biol. (2011), https://doi.org/10.1083/jcb.201007108.
[30] F.X. Yu, B. Zhao, N. Panupinthu, J.L. Jewell, I. Lian, L.H. Wang, J. Zhao, H. Yuan, K. Tumaneng, H. Li, X.D. Fu, G.B. Mills, K.L. Guan, Regulation of the Hippo-YAP Pathway by G-Protein-Coupled Receptor Signaling, Cell, (2012), https://doi.org/10.1016/j.cell.2012.06.037.
[31] J.X. Pan, L. Xiong, K. Zhao, P. Zeng, B. Wang, F.L. Tang, D. Sun, H.H. Guo, X. Yang, S. Cui, W.F. Xia, L. Mei, W.C. Xiong, YAP Promotes Osteogenesis and Suppresses Adipogenic Differentiation by Regulating β-Catenin Signaling, Bone Res, (2018), https://doi.org/10.1038/s41413-018-0018-7.
[32] L.F. Bonewald, The role of the osteocyte in Bone and nonbone disease, Endocrinol. Metab. Clin. N. Am. (2017), https://doi.org/10.1016/j.ecl.2016.09.003.
[33] K.A. Staines, B. Javaheri, P. Hohenstein, R. Fleming, E. Ikpegbu, E. Unger, M. Hopkinson, D.J. Buttle, A.A. Pitsillides, C. Farquharson, Hypomorphic conditional deletion of E11/Podoplanin reveals a role in osteocyte dendrite elongation, J. Cell. Physiol. (2017), https://doi.org/10.1002/jcp.25999.
[34] M. Ai, S.L. Holmen, W. Van Hul, B.O. Williams, M.L. Warman, Reduced affinity to and inhibition by DKK1 form a common mechanism by which high bone mass-associated missense mutations in LRP5 affect canonical Wnt signaling, Mol. Cell. Biol. (2005), https://doi.org/10.1128/mcb.25.12.4946-4955.2005.
[35] S.L. Dallas, M. Prideaux, L.F. Bonewald, The osteocyte: an endocrine cell … and more, Endocr Rev. (2013), https://doi.org/10.1210/er.2012-1026.
[36] E. Ikpegbu, L. Basta, D.N. Clements, R. Fleming, T.L. Vincent, D.J. Buttle, A.A. Pitsillides, K.A. Staines, C. Farquharson, FGF-2 promotes osteocyte differentiation through increased E11/podoplanin expression, J. Cell. Physiol. (2018), https://doi.org/10.1002/jcp.26345.
[37] J. Chen, Y. Shi, J. Regan, K. Karuppaiah, D.M. Ornitz, F. Long, Osx-Cre Targets Multiple Cell Types besides Osteoblast Lineage in Postnatal Mice, PloS One, (2014), https://doi.org/10.1371/journal.pone.0085161.
[38] J.P. Mansell, M. Nowghani, M. Pabbruwe, I.C. Paterson, A.J. Smith, A.W. Blom, Lysophosphatidic Acid and Calcitriol Co-Operate to Promote Human Osteoblastogenesis: Requirement of Albumin-Bound LPA, Prostaglandins Other Lipid Mediat, (2011), https://doi.org/10.1016/j.prostaglandins.2011.05.003.
[39] C.D. Kegelman, D.E. Mason, J.H. Dawahare, D.J. Horan, G.D. Vigil, S.S. Howard, A.G. Robling, T.M. Bellido, J.D. Boerckel, Skeletal Cell YAP and TAZ Combinatorially Promote Bone Development, Faseb J, (2018), https://doi.org/10.1096/fj.201700872R.
[40] C.D. Kegelman, J.C. Coulombe, K.M. Jordan, D.J. Horan, L. Qin, A.G. Robling, V.L. Ferguson, T.M. Bellido, J.D. Boerckel, YAP and TAZ Mediate Osteocyte Perilacunar/Canalicular Remodeling, J. Bone. Miner, Res, 2020, https://doi.org/10.1002/jbmr.3876.
[41] D. Yasuda, D. Kobayashi, N. Akahoshi, T. Ohto-Nakanishi, K. Yoshioka, Y. Takuwa, S. Mizuno, S. Takahashi, S. Ishii, Lysophosphatidic acid-induced YAP/TAZ activation promotes developmental angiogenesis by repressing notch ligand Dll4, J. Clin. Invest. (2019), https://doi.org/10.1172/jci121955.
[42] Y.B. Liu, Y. Kharode, P.V. Bodine, P.J. Yaworsky, J.A. Robinson, J. Billiard, LPA induces osteoblast differentiation through interplay of two receptors: LPA1 and LPA4, J. Cell. Biochem. (2010), https://doi.org/10.1002/jcb.22471.
[43] J.P. Salles, S. Laurencin-Dalicieux, F. Conte-Auriol, F. Briand-Mesange, I. Gennero, Bone defects in LPA receptor genetically modified mice, Biochim. Biophys. Acta (2013), https://doi.org/10.1016/j.bbalip.2012.07.018.
[44] S.K. Murali, O. Andrukhova, E.L. Clinkenbeard, K.E. White, R.G. Erben, Excessive osteocytic Fgf23 secretion contributes to pyrophosphate accumulation and mineralization defect in Hyp Mice, PLoS Biol. (2016), https://doi.org/10.1371/journal.

pbio.1002427.
[45] D.R. Eyre, M.A. Weis, Bone collagen: new clues to its mineralization mechanism from recessive osteogenesis imperfecta, Calcif. tissue Int. (2013), https://doi.org/10.1007/s00223-013-9723-9.
[46] D.B. Burr, Changes in Bone Matrix Properties with Aging, Bone, (2019), https://doi.org/10.1016/j.bone.2018.10.010.
[47] M.H. Sheng, D.J. Baylink, W.G. Beamer, L.R. Donahue, C.J. Rosen, K.H. Lau, J.E. Wergedal, Histomorphometric Studies Show that Bone Formation and Bone Mineral Apposition Rates Are Greater in C3H/HeJ (High-Density) than C57BL/6J (Low-Density) Mice during Growth, Bone, (1999), https://doi.org/10.1016/s8756-3282(99)00184-2.
[48] J.N. Farr, D.G. Fraser, H. Wang, K. Jaehn, M.B. Ogrodnik, M.M. Weivoda, M.T. Drake, T. Tchkonia, N.K. LeBrasseur, J.L. Kirkland, L.F. Bonewald, R.J. Pignolo, D.G. Monroe, S. Khosla, Identification of Senescent Cells in the Bone Microenvironment, J. Bone. Miner, Res, 2016, https://doi.org/10.1002/jbmr.2892.
[49] C.M. Andreasen, J.M. Delaisse, B.C.J. van der Eerden, J. van Leeuwen, M. Ding, T.L. Andersen, Understanding Age-Induced Cortical Porosity in Women: Is a Negative BMU Balance in Quiescent Osteons a Major Contributor? Bone, (2018), https://doi.org/10.1016/j.bone.2018.09.011.
[50] W. Bouleftour, L. Juignet, G. Bouet, R.N. Granito, A. Vanden-Bossche, N. Laroche, J.E. Aubin, M.H. Lafage-Proust, L. Vico, L. Malaval, The Role of the SIBLING, Bone Sialoprotein in Skeletal Biology - Contribution of Mouse Experimental Genetics, Matrix Biol, (2016), https://doi.org/10.1016/j.matbio.2015.12.011.
[51] D. Tokarz, J.S. Martins, E.T. Petit, C.P. Lin, M.B. Demay, E.S. Liu, Hormonal Regulation of Osteocyte Perilacunar and Canalicular Remodeling in the Hyp Mouse Model of X-Linked Hypophosphatemia, J. Bone. Miner, Res, 2018, https://doi.org/10.1002/jbmr.3327.
[52] L.F. Bonewald, The Amazing Osteocyte, J. Bone. Miner, Res, 2011, https://doi.org/10.1002/jbmr.320.
[53] A. Grey, Q. Chen, K. Callon, X. Xu, I.R. Reid, J. Cornish, The Phospholipids Sphingosine-1-Phosphate and Lysophosphatidic Acid Prevent Apoptosis in Osteoblastic Cells Via a Signaling Pathway Involving G(I) Proteins and Phosphatidylinositol-3 Kinase, Endocrinol, (2002), https://doi.org/10.1210/en.2002-220347.
[54] S. Yao, Y. Zhang, X. Wang, F. Zhao, M. Sun, X. Zheng, H. Dong, K. Guo, Pigment epithelium-derived factor (PEDF) protects Osteoblastic cell line from glucocorticoid-induced apoptosis via PEDF-R, Int. J. Mol. Sci. (2016), https://doi.org/10.3390/ijms17050730.
[55] X. Li, M.S. Ominsky, Q.T. Niu, N. Sun, B. Daugherty, D. D'Agostin, C. Kurahara, Y. Gao, J. Cao, J. Gong, F. Asuncion, M. Barrero, K. Warmington, D. Dwyer, M. Stolina, S. Morony, I. Sarosi, P.J. Kostenuik, D.L. Lacey, W.S. Simonet, H.Z. Ke, C. Paszty, Targeted Deletion of the Sclerostin Gene in Mice Results in Increased Bone Formation and Bone Strength, J. Bone. Miner, Res, 2008, https://doi.org/10.1359/jbmr.080216.
[56] P. Chavassieux, R. Chapurlat, N. Portero-Muzy, J.P. Roux, P. Garcia, J.P. Brown, C. Libanati, R.W. Boyce, A. Wang, A. Grauer, Bone-Forming and Antiresorptive Effects of Romosozumab in Postmenopausal Women with Osteoporosis: Bone Histomorphometry and Microcomputed Tomography Analysis after 2 and 12 Months of Treatment, J. Bone. Miner, Res, 2019, https://doi.org/10.1002/jbmr.3735.
[57] C. Sanchez-de-Diego, N. Artigas, C. Pimenta-Lopes, J.A. Valer, B. Torrejon, P. Gama-Perez, J.A. Villena, P.M. Garcia-Roves, J.L. Rosa, F. Ventura, Glucose Restriction Promotes Osteocyte Specification by Activating a PGC-1alpha-Dependent Transcriptional Program, iScience, (2019), https://doi.org/10.1016/j.isci.2019.04.015.
[58] K.M. Waters, J.M. Jacobs, M.A. Gritsenko, N.J. Karin, Regulation of Gene Expression and Subcellular Protein Distribution in MLO-Y4 Osteocytic Cells by Lysophosphatidic Acid: Relevance to Dendrite Outgrowth, Bone, (2011), https://doi.org/10.1016/j.bone.2011.02.020.